2018 IEEE International Conference on Robotics and Automation (ICRA)
May 21-25, 2018, Brisbane, Australia

A Tensegrity-Inspired Compliant 3-DOF Compliant Joint

Jeffrey M. Friesen[1], John L. Dean[2], Thomas Bewley[1], Vytas Sunspiral[3]

Abstract— **Our Tensegrity-Inspired Compliant Three degree-of-freedom (DOF) robotic joint adds omnidirectional compliance to robotic limbs while reducing sprung mass through base mounted actuation. This enables a robotic limb which is safer to operate alongside humans and fragile equipment while still capable of generating quick movements and large forces if required. Unlike many other soft robotic systems which leverage continuously soft materials, our joint is simpler to model with low order dynamic systems and has a host of embedded sensing which provide ample information of its position and velocity. We first discuss geometry selection and optimization to maximize the theoretical configuration space of the joint. We then show several of our mechatronic design solutions, which are easily generalized to a multitude of cable-driven mechanisms, and demonstrate the performance of these mechanisms within the context of our hardware prototype. We then present results on the controllable stiffness of our physical prototype. Finally, we demonstrate the strength of our prototype which is capable of lifting a 7 kg mass at a distance of 0.95 meters from the joint.**

Fig. 1. A picture of our 3 DOF Joint within a robotic arm assembly. On the top right is a simplified model of our joint shown in the same orientation, showing the connectivity of the topology for clarification.

I. INTRODUCTION

Robotics and automation has revolutionized much of the manufacturing industry today, with robots able to perform many tasks more efficiently and consistently than a human. However, much of the technology developed to enable this cannot function safely or effectively outside of the structured factory environments and separate from people and other unpredictable systems. One application where this is critical is in space robotics; such robots need to operate effectively alongside fragile equipment and astronauts, and need to offer guarantees on limited force transfer for safety reasons. These robots will also need to be capable of applying accurate, consistent and concentrated forces while still maintaining some adaptability for uncertainties in the environment.

One approach taken to address these challenges is to augment traditional rigid robotic systems with a range of force sensing capabilities and series elastic actuators combined with advanced software to monitor environmental interactions verse planned trajectories to mitigate undesired contacts. One example of this in a space robotics application is Robonaut 2 [1].This can result in robots with many of the impressive characteristics of factory robots capable of precise motion while avoiding unsafe contact with the environment. Such systems are safe when all software and sensors function correctly and accurately, but inevitably software bugs or hardware failures can result in dangerous situations for the robot and any nearby objects or people.

Soft robotics offers interesting solutions to these challenges through the integration of low-durometer materials. Examples of such systems include work on a soft pneumatic arm [2] and a soft tentacle inspired manipulator [3]. There are still major design challenges that these systems need to address before they can produce robots with comparable capabilities to their rigid counterparts. The first of these is accurate real-time modeling, which is challenging due to the continuously deformable materials used which often have time-dependent mechanical properties and require a high number of finite elements to describe their behavior accurately. The second challenge is sensor integration as many off-the-shelf sensing solutions do not integrate easily into soft systems. A final difficulty of fully soft systems is when a task requires large concentrated and localized forces to be applied for completion such as pressing a stiff button, pulling a rope, or lifting a dense object.

We propose to leverage tensegrity principles to create robotic systems which have discretized softness with granular rigidity. Tensegrity is a structural paradigm in which rigid elements are suspended in a network of tension elements [4]. Such structures pass all loading through pure compression or tension, producing a mass efficient structure with inherent compliance [5], [6]. Much work has been done to leverage

*This work was supported by a NASA Space Technology Research Fellowship, and also NASA's Human Robotic Systems (HRS) project, Game Changing Developments (GCD) Program, Space Technology Mission Directorate (STMD)

[1]Jeffrey Friesen and Thomas Bewley are with the UC San Diego Coordinated Robotics Lab, MC 0411, La Jolla CA, 92093 USA jfriesen@ucsd.edu, bewley@ucsd.edu

[2]John L. Dean is with Stanford University 350 Serra Mall Stanford, CA 94305-9505 DeanJL@Stanford.edu

[3]Vytas Sunspiral was a Senior Robotics Researcher, SGT Inc., with the Intelligent Robotics Group, NASA Ames Research Center, Moffett Field CA 94035 USA vytas.sunspiral@gmail.org

these tensegrity properties and realize them in robotic systems but more work needs to be done to improve the performance of these initial efforts [7], [8], [9]. We will show that such systems can benefit from easier modeling and sensor integration while maintaining some of the adaptability and safety of soft systems. Additionally, tensegrity systems can offer tunable stiffness allowing for the targeted application of large forces when needed and compliant passive behavior when adaptability is more favored.

We first discuss our design process for the topology and geometry of our proposed joint. We then focus on the mechanical design of our prototype to demonstrate real world performance and introduce several mechanism which enable this. Our design includes embedded series compliance mechanisms with integrated force sensing, allowing for detection of cable-slack conditions as well as enabling the calculation of external joint forces. We show our cable-routing mechanism which includes additional embedded sensing to ascertain one component of cable direction, information which will be valuable for state estimation similar to [10]. We demonstrate that the prototype is capable of handling large loading, lifting 70 Newtons of weight at a distance of 0.95 meters from the joint. We also demonstrate its controllable external stiffness through a preliminary experiment. Finally, we discuss future research directions now that we have a fully functional mechanical prototype for testing.

II. Joint Topology Analysis

The first challenge we addressed was topology selection. We focused on selecting a geometry with a broad and convex workspace to allow for the combined rotations required for smooth motion of the robotic limb. Due to space constraints, we cannot offer a complete description of all details of the optimization described below, however all MATLAB code used in this analysis is accessible via the git repository located at [11].

A. Workspace Analysis

We identified several tools for efficiently computing the configuration space of a cable-driven joint, so we could quickly evaluate different joint topologies. While many approaches to defining the workspace of a parallel robot exist [12], [13], [14], we found success with the approach from Pham et al. which outlines a Force Closure Check (FCC) method for checking for the force closure property, a property commonly used in systems with unidirectional forcing. Force closure guarantees that the system can resist any external force or moment given infinite actuator force [15]. They used this algorithm to characterize the workspace of several candidate geometries.

We took inspiration from the shoulder joint topology proposed in [16] and replaced the ball-and-socket in their joint with a system of three saddle cables defined in fig. 3. Replacing the ball joint makes the integration of translational compliance through elasticity in the saddle cables possible. If only rotational motion across the joint is desired, these three cables can remain passive, requiring only six actuated

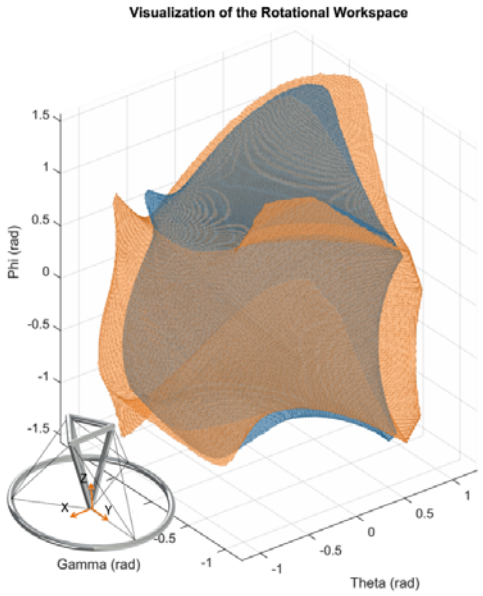

Fig. 2. The optimized joint topology is shown at the bottom left with the designation of the body-fixed coordinate system. The plot shows a comparison between the workspace of the optimized joint topology (orange) and an initial selected joint geometry (blue). Note that Phi, Gamma and Theta represent Euler Rotations about the body fixed coordinates X, Y, and Z respectively. Any point within the shape is within the workspace of the joint geometry.

cables. An additional reason for this replacement is to avoid the mechanical complexity that comes with the design of a large range-of-motion 3-DOF ball joint.

Our implementation of the FCC algorithm in [15] yielded results but took a large amount of time to execute. We suspect this is due to MATLAB inefficiently handling the recursive function used in the FCC algorithm. Instead, we replaced the recursive method with an openly available MATLAB function, inHull [17], capable of efficiently checking if a point is contained in a convex hull effectively in n dimensions.

We selected some geometric parameters for our joint topology and characterized its workspace, shown in blue in fig. 2. We found that the geometry of our our joint was difficult to tune by hand, and with an easy and efficient algorithm on hand for characterizing the workspace we opted to instead perform an optimization over these parameters to maximize the workspace of our joint topology.

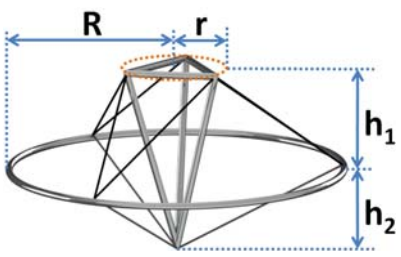

Fig. 3. Here the joint is depicted with an axially symmetric parametrization of its geometry used within our optimization. Note that what we describe as saddle cables are the three cable which connect from the ring to the lower central node of the tetrahedron in this diagram.

B. Topology Optimization

We selected a geometric parametrization with four independent values, which maintained radial symmetry of the joint shown in fig. 3. We then created a uniform grid of rotational orientations to ensure equal weighting of different configurations. This was achieved using quaternions specified by Hopf Fibration, a mapping which parametrizes the four dimensional sphere as a three-dimensional sphere and a circle, which allows known discretizations of the one sphere (a circle) and two sphere to be used to produce a uniform mapping of the three sphere [18]. Our modified force closure check algorithm was then evaluated along a discretized set of approximately 80,000 uniformly spaced orientations for a given geometry. The resultant sum of possible configurations was used as an integer valued cost function. Note that an additional check for self-intersecting geometry was also used to ensure feasibility of a given configuration.

Because the output of our cost function is integer valued and discontinuous, gradient based optimization methods cannot be used. Instead we used the generalized pattern search algorithm provided with the optimization toolbox in MATLAB. This proved effective and converged over the course of several hundred function evaluations. Depending on the number of joint orientations tested, typically between two thousand and eighty thousand, the optimization took between a half hour and several days to converge. We also tested from multiple initial conditions in an attempt to avoid local minima, and found the algorithm consistently converged to the same point within a margin of tenths of millimeters if a higher number of joint orientations was used.

The workspace of the resultant geometry produced by this optimization is depicted in fig. 2, and compared against our initial hand-tuned geometry. It is seen we achieve a significant improvement in the volume of the feasible workspace.

Param.	Lower Bound	Upper Bound	Optimized
R	15 cm	15 cm	15 cm
r	3 cm	17 cm	4.78 cm
h_1	15 cm	60 cm	16.52 cm
h_2	1 cm	10 cm	2.35 cm

III. Cable Actuation Architecture

Having force closure at all equilibrium positions of the joint guarantees that we can find a set of cable-tensions to resist any external force or moment applied across the joint. If we can measure both the current configuration of the joint as well as the forces within the cables, we can monitor and control all forces and moments across the joint. Furthermore, if we can tune the apparent mechanical stiffness of the cables, we can change the external stiffness of the joint for different types of manipulation tasks. Here we outline our control approach to enable controllable stiffness of the cables and outline the host of sensors and mechanisms which enable this control to be realized within our physical prototype.

For the current prototype, each of the six outer cables is augmented with identical sensing and actuation. All saddle cables are left passive with no sensing, as they effectively serve as a ball-and-socket within the joint.

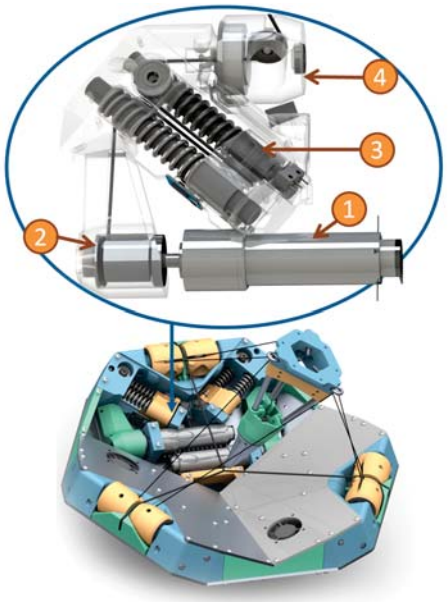

Fig. 4. Below we have a render of the mechanical layout of the joint with one face-plate removed to show two cable actuators. The total system mass for this design is 4.3 kilograms. Above we see a close up of the cable routing mechanism. A DC Maxon motor (1) is affixed with an aluminum pulley (2). A cable is spooled on this cable and fed through the series compliance mechanism (3) where it then exits the assembly through the omnidirectional cable-routing mechanism (4).

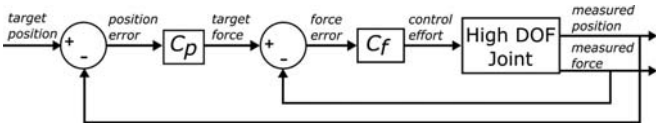

Fig. 5. Feedback control diagram for the low level cable controller. The Target position is supplied by the high level controller. Cp is the proportional controller for position, which feeds Cf, a proportional controller for force. This creates a linear spring behaviour for low frequency (less than 100 Hz) disturbances in the closed loop system. Both the position and force measurements are obtained through encoders.

A. Low-Level Cable Control

For high level control of the system, an assumption of linear cable stiffness makes dynamic modeling simpler as compared to cables with non-linear behaviour. Additionally, a variable stiffness is required for the joint to be applicable in different environments requiring a range of compliance. Since a simple passive mechanism cannot achieve both of these, a low level cable controller is necessary. Fig. 5 shows the control diagram for the low level cable controller.

One difficulty in achieving a good approximation of linear stiffness with the controller is obtaining an accurate force measurement. We achieve this through the implementation of series-compliance force sensors and low friction cable routing. Additionally, the controller must operate at a high enough frequency to provide smoothing for velocity estimates based on our position sensors. This is achieved using a centralized embedded system design which we describe

below.

B. Cable Mechanism

Fig. 4 shows an overview of our cable-drive system, which is identical for each of the six actuated cables in our joint. A 20 Watt DCX Maxon motor with a 72:1 gearbox affixed with an 18 millimeter diameter spool is used for actuation of the cable. This system is capable of generating over 400 Newtons of cable-tension, and a maximum cable speed of approximately 10 cm/s. This motor is also equipped with an encoder to track the amount of cable spooled. After leaving the spool, the cable is fed through a series of mechanisms for sensing and routing described below.

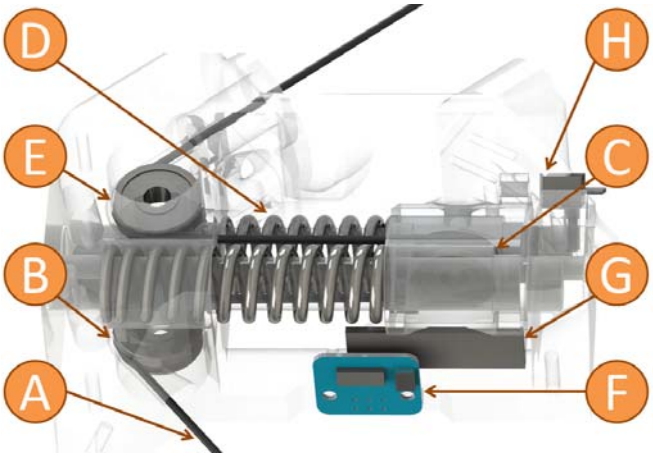

Fig. 6. Depicted above is our series compliance mechanism. The cable (A) enters from the motor spool and wraps around fixed pulley (B) then continues to moving pulley (C) which is attached to compression springs (D). The cable continues over fixed pulley (E) and exits toward the omnidirectional routing mechanism. Magnetic encoder sensor (F) and magnetic strip (G) provide spring displacement measures with limit switch (H) giving an absolute reference.

An accurate and consistent cable-tension measurement is required to effectively implement our cable control strategy. This desired measurement is non-trivial to implement mechanically [19]. Our solution consists of a series compliance mechanism depicted in Fig. 6. The cable is routed over a series of three pulleys, with the middle pulley affixed to a linear slider whose motion compresses two linear compression springs. Two identical springs are used to balance all forces within the mechanism which prevents jamming in the linear slider mechanism.

This linear slider is affixed with a position sensor which yields a measure of spring displacement used to estimate cable force. While the bandwidth of this sensor will be lower when compared against a strain-gauge based solution, it is still adequate for our application. The mass of the linear slider component is roughly 30 grams while the spring stiffness is 29 kN/m. This yields a response frequency of roughly 1 kHz which should be sufficient for our application. Results from a static test of the force sensor are shown in fig. 8. An additional benefit is that the stiffness of this mechanism is significantly lower than the varying and time dependent stiffness of the HDPE cables of the robot

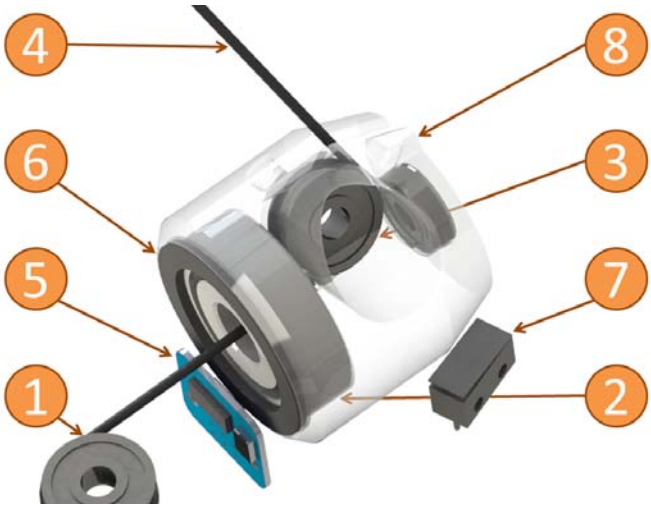

Fig. 7. Depicted above is the omnidirectional cable routing mechanism. The cable (1) enters from the series compliance mechanism passes through axial/thrust bearing (2) before passing over pulley (3) which can passively rotate about the axis of bearing (2). The cable exit (4) is then able to point in arbitrary directions as the pulley (3) follows the cable direction. Magnetic encoder sensor (5) and magnetic ring (6) track the angle of the cable exit with limit switch (7) providing an absolute displacement when it makes contact with nub (8).

(greater than 300 kN/m), meaning the cable stiffness can be accurately estimated as a constant 29 kN/m simplifying system dynamics [20].

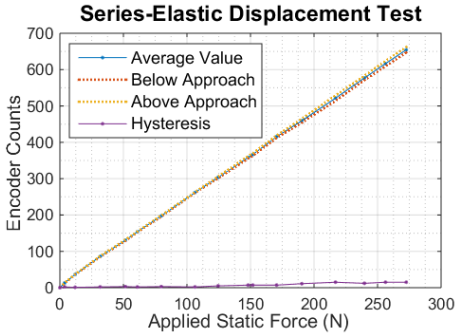

Fig. 8. Here we show results from a static test of our series compliance force sensing. The below average data was collected by gently resting a known proof mass onto the cable, while above average values were measured by overloading the cable and then gently removing the extra force. The hysteresis line depicts the difference between these two lines.

After leaving the series compliance mechanism the cable must be routed out to the joint whose relative position changes depending on the current joint position. Smooth eyelets are a common but inadequate solution to this cable routing problem, and fail to effectively mitigate friction. Any friction at the cable exit point will contribute undesirable hysteresis to our force measurements, reduce the efficiency of the mechanism, and cause unacceptable levels of cable wear.

Instead we have designed an omnidirectional cable routing mechanism (Fig. 7), consisting of a pulley mounted to a bearing, wherein the bearings axis is in line with the path of the cable entering the pulley. As the cable changes direction,

the pulley will passively follow the perpendicular component of the cable direction while the second component of cable direction can be accounted for by wrapping or unwrapping onto the pulley, thus passing all loading from redirection over a passive pulley. This eliminates the majority of cable friction at the exit point. One drawback is the cable exit point has a more complicated kinematic relationship to the mechanism positioning [21]. Fortunately, an angle measurement of this mechanism is straightforward to sense, and yields one component of cable direction relative to the joint.

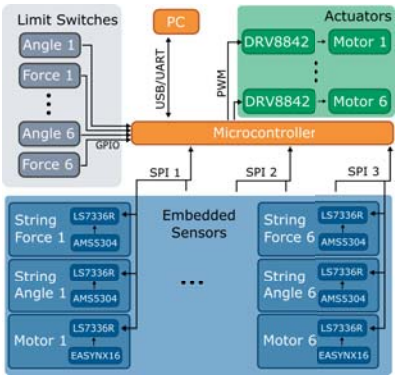

Fig. 9. Information flow diagram for embedded system. The string rest length is determined by the Maxon ENX 16 encoder embedded with the motors. The string angle and string force are both determined by the AMS5304 multi-pole magnetic strip position sensor. Each of these signals are counted by the LS7336R encoder counters, which communicate with the dsPIC33 through 3 parallel SPI buses. The limit switches connect to GPIO pins on the dsPIC.

In total, our design incorporates eighteen quadrature encoder signals to track six tension sensors, six cable angle sensors, and six motor positions. This, combined with the need for a relatively high control frequency, places stringent real-time requirements on our embedded system. As a decentralized network of microcontrollers would be challenging to synchronize, we have utilized a dedicated quadrature decoder IC which tracks the quadrature signals from each sensor, and communicates with the single microcontroller over an SPI interface. The information flow diagram for the system is shown in fig. 9.

IV. Initial Tests of the Physical Prototype

We performed several preliminary tests to demonstrate the mechanical performance of our hardware prototype. We implemented an inverse kinematic (IK) control policy via the force density method as outlined in [22], [23], and [24] as a simple open-loop controller for sending static commands to the joint. This controller assumes known external forces, and for all tests conducted here all external forces were set to zero.

For testing, the joint was rigidly mounted to a lab bench with an attached aluminum arm as shown in fig. 11. The first test demonstrates the controllable stiffness of the joint. A 1.2 kg proof mass was affixed to the end of a 0.95 meter arm while the joint was commanded with the IK controller to hold the arm parallel to the ground. The weight was then lifted

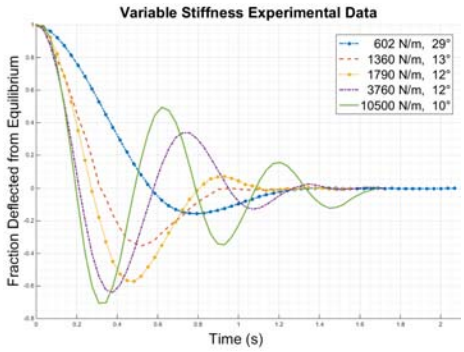

Fig. 10. This is a plot showing a series of experiments exciting the prototype with step disturbances. The plot was normalized for clarity, but the amplitude of angular displacement before normalization is shown in the legend. This data demonstrate the controllable stiffness of the joint.

Fig. 11. The joint was affixed with a HEBI X-series actuator to serve as an elbow with a 1.2 kg proof mass attached (above). The arm was then held up by our joint while the elbow was held at a right angle. Our joint was then used to lift the proof mass demonstrating it's ability to apply a torsional moment of 6 Newton-meters. Next the joint was affixed with a 95cm rigid arm (below) and a proof mass of 7 kilograms. In this configuration the prototype was able to lift the mass with a maximum cable-tension of 310 Newtons to apply a 65 Newton-meter torque.

to a small angular displacement and dropped. The resulting excitation of the arm was tracked with color markers and video post-processing. The data was normalized according to amplitude of the step disturbance and equilibrium position. Results of this test are depicted in fig. 10.

Multiple trials are depicted with varied target stiffness of the position controller. The highest resonant frequency shown is 1.5 Hz and the lowest is 0.6 Hz, showing a 2.5 times increase in resonant frequency demonstrating the controllable stiffness of the joint. The results of this test demonstrate that the natural frequency, and thus the external stiffness of the system, is able to be actively controlled by tuning the constants of our low level controllers.

The second test demonstrates the strength of the joint, and is described in fig. 11. This demonstrates that the strength of the joint is comparable to the strength of other state of the art humanoid robotic shoulders such as Robonaut 2, whose

arm is capable of lifting 90 Newtons at a distance of 0.8 meters [25], [1].

V. Future Work

We have proposed a new joint topology and optimized its workspace with respect to its geometry. We then designed and fabricated a mechanical prototype using this topology, and demonstrated some of its basic capabilities with simple tests using an IK controller. We explained the mechanisms and sensors within the prototype which enable it to operate effectively. These mechanisms are straightforward to adapt to improve other cable driven robotic systems. We believe the parallel cable-driven joint presented here offers a balanced design that reduces limb inertia, allows for controllable compliance and and offers a large convex workspace as compared to other existing compliant robotic joint designs.

Further work needs to be done for workspace optimization. An indexed optimization using both the workspace size as well as its positioning accuracy could produce better results for the optimized topology. Additionally other methods of force flosure analysis could create more accurate representations of the joint workspace by accounting for factors such as slack cables which were not analyzed here.

Additionally while our current mechanical prototype offers some initial insight into these advantages, we need to integrate the system more tightly with a control scheme to fully demonstrate its abilities. We also need to more thoroughly analyze the prototypes abilities in different orientations, and test the range of its speed and stiffness within its workspace. Furthermore, more evaluation of the joint needs to be done to directly compare the joint with other existing robotic joints.

Our next steps are implementing a state estimation technique coupled with a state feedback controller to effectively leverage this capable hardware. We will then work to implement control techniques which are capable of independently controlling position and stiffness about each rotational axis of the joint.

VI. Acknowledgments

We appreciate the support, ideas, and feedback from members of the Dynamic Tensegrity Robotics Lab: Ken Caluwaerts, Jonathan Bruce, and Steven Lessard. We also appreciate the support from Terry Fong and the Intelligent Robotics Group at NASA Ames Research Center in further enabling this research. We would also like to thank HEBI robotics for lending us one of their X-Series Industrial Actuators to use within our experimental setup. Lastly we would like to thank NVIDIA Corporation for the hardware donation which enabled us to CAD efficiently.

References

[1] M. A. Diftler, J. Mehling, M. E. Abdallah, N. A. Radford, L. B. Bridgwater, A. M. Sanders, R. S. Askew, D. M. Linn, J. D. Yamokoski, F. Permenter, *et al.*, "Robonaut 2-the first humanoid robot in space," in *Robotics and Automation (ICRA), 2011 IEEE International Conference on*. IEEE, 2011, pp. 2178–2183.

[2] S. Sanan, P. S. Lynn, and S. T. Griffith, "Pneumatic torsional actuators for inflatable robots," *Journal of Mechanisms and Robotics*, vol. 6, no. 3, p. 031003, 2014.

[3] B. Mazzolai, L. Margheri, M. Cianchetti, P. Dario, and C. Laschi, "Soft-robotic arm inspired by the octopus: Ii. from artificial requirements to innovative technological solutions," *Bioinspiration & biomimetics*, vol. 7, no. 2, p. 025005, 2012.

[4] S. Levin, "Tensegrity: the new biomechanics," *Textbook of musculoskeletal medicine*, vol. 9, 2006.

[5] R. E. Skelton and M. C. Oliveira, *Tensegrity systems*. Springer, 2009.

[6] R. E. Skelton, R. Adhikari, J.-P. Pinaud, W. Chan, and J. Helton, "An introduction to the mechanics of tensegrity structures," in *Decision and Control, 2001. Proceedings of the 40th IEEE Conference on*, vol. 5. IEEE, 2001, pp. 4254–4259.

[7] S. Lessard, D. Castro, W. Asper, S. D. Chopra, L. B. Baltaxe-Admony, M. Teodorescu, V. SunSpiral, and A. Agogino, "A bio-inspired tensegrity manipulator with multi-dof, structurally compliant joints," *arXiv preprint arXiv:1604.08667*, 2016.

[8] K. Caluwaerts, J. Despraz, A. Işçen, A. P. Sabelhaus, J. Bruce, B. Schrauwen, and V. SunSpiral, "Design and control of compliant tensegrity robots through simulation and hardware validation," *Journal of The Royal Society Interface*, vol. 11, no. 98, 2014. [Online]. Available: http://dx.doi.org/10.1098/rsif.2014.0520

[9] T. Bliss, T. Iwasaki, and H. Bart-Smith, "Central pattern generator control of a tensegrity swimmer," *IEEE/ASME Transactions on Mechatronics*, vol. 18, no. 2, pp. 586–597, 2013.

[10] K. Caluwaerts, J. Bruce, J. M. Friesen, and V. SunSpiral, "State estimation for tensegrity robots," in *2016 IEEE International Conference on Robotics and Automation (ICRA)*, May 2016, pp. 1860–1865.

[11] Joint optimization git repository. [Online]. Available: https://github.com/Jfriesen222/Joint_Workspace_Analysis

[12] M. Gouttefarde, D. Daney, and J.-P. Merlet, "Interval-analysis-based determination of the wrench-feasible workspace of parallel cable-driven robots," *IEEE Transactions on Robotics*, vol. 27, no. 1, pp. 1–13, 2011.

[13] D. Lau, D. Oetomo, and S. K. Halgamuge, "Wrench-closure workspace generation for cable driven parallel manipulators using a hybrid analytical-numerical approach," *Journal of Mechanical Design*, vol. 133, no. 7, p. 071004, 2011.

[14] W. B. Lim, G. Yang, S. H. Yeo, and S. K. Mustafa, "A generic force-closure analysis algorithm for cable-driven parallel manipulators," *Mechanism and Machine Theory*, vol. 46, no. 9, pp. 1265–1275, 2011.

[15] C. B. Pham, S. H. Yeo, G. Yang, M. S. Kurbanhusen, and I.-M. Chen, "Force-closure workspace analysis of cable-driven parallel mechanisms," *Mechanism and Machine Theory*, vol. 41, no. 1, pp. 53–69, 2006.

[16] S. Lansdberger and T. Sheridan, "A new design for parallel link manipulators," in *Proc. Sys. Man. and Cybernetics Conf., Tucson, AZ*, 1985, pp. 812–814.

[17] Matlab inhull function. [Online]. Available: https://www.mathworks.com/matlabcentral/fileexchange/10226-inhull

[18] A. Yershova, S. Jain, S. M. Lavalle, and J. C. Mitchell, "Generating uniform incremental grids on so (3) using the hopf fibration," *The International journal of robotics research*, 2009.

[19] W. Kraus, M. Kessler, and A. Pott, "Pulley friction compensation for winch-integrated cable force measurement and verification on a cable-driven parallel robot," in *Robotics and Automation (ICRA), 2015 IEEE International Conference on*. IEEE, 2015, pp. 1627–1632.

[20] J.-P. Merlet, "The influence of discrete-time control on the kinematico-static behavior of cable-driven parallel robot with elastic cables," in *Advances in Robot Kinematics*. Springer, 2014, pp. 113–121.

[21] A. Pott, "Influence of pulley kinematics on cable-driven parallel robots," in *Latest Advances in Robot Kinematics*. Springer, 2012, pp. 197–204.

[22] J. Friesen, A. Pogue, T. Bewley, M. de Oliveira, R. Skelton, and V. Sunspiral, "Ductt: A tensegrity robot for exploring duct systems," in *Robotics and Automation (ICRA), 2014 IEEE International Conference on*. IEEE, 2014, pp. 4222–4228.

[23] J. M. Friesen, P. Glick, M. Fanton, P. Manovi, A. Xydes, T. Bewley, and V. Sunspiral, "The second generation prototype of a duct climbing tensegrity robot, ducttv2," in *2016 IEEE International Conference on Robotics and Automation (ICRA)*. IEEE, 2016, pp. 2123–2128.

[24] H.-J. Schek, "The force density method for form finding and computation of general networks," *Computer Methods in Applied Mechanics and Engineering*, vol. 3, no. 1, pp. 115 – 134, 1974. [Online]. Available: http://www.sciencedirect.com/science/article/pii/0045782574900450

[25] Robonaut 2 fact sheet. [Online]. Available: https://www.nasa.gov/sites/default/files/files/Robonaut2_508.pdf